Acta Polytechnica CTU Proceedings **33**:284–289, 2022
https://doi.org/10.14311/APP.2022.33.0284

Published by the Czech Technical University in Prague

LOWER BOUND ANALYSIS FOR SHEAR ASSESSMENT OF FULL-SCALE RC GIRDERS SUBJECTED TO AXIAL TENSION

Takeru Kanazawa

Hokkai Gakuen University, 1-1, Minami 26, Nishi 11, Tyuo-ku, Sapppro, Hokkaido, Japan
correspondence: t-kanazawa@hgu.jp

Abstract.

Axial tension force exerted as a result of a temperature change or shrinkage can cause the collapse of RC structural members. Design code provisions and analytical models such as Modified Compression Field Theory (MCFT) yield reasonable estimates of shear strength of RC beams subjected to axial tension. Nevertheless, their semi-empirical nature is not necessarily appropriate for shear assessment of existing RC structural members. The extra conservativeness and empirically determined parameters might require unnecessary maintenance work. A generalised model with rigorous formulation must be developed. This paper presents a purely theoretical model to predict the shear strength of RC beams under axial tension based on limit analysis. Without regressive functions and empirical functions, lower bound analysis enables shear strength derivation when the force equilibrium and strain compatibility are satisfied. Accuracy of the analysis was verified by comparison of its predictions with three experimental shear strengths of full-scale RC girders. An equal level of accuracy was observed between the analytical solutions and MCFT-based predictions.

Keywords: Axial tension, full-scale RC girders, lower bound analysis, shear assessment.

1. Introduction

The sustainability of RC structures is an important issue worldwide because of their exposure to a variety of loading with environmental and mechanical actions. The partial collapse of the Wilkins Air Force Depot in 1955 [1] spurred the refinement of design practices for shear under axial tension caused by a temperature change or shrinkage. The brittle collapse was reproduced in laboratory investigation [1]. Results demonstrated that tensile stress of approximately 1.4 N/mm^2 can reduce shear strength by 50% [2]. Design code provisions have difficulty in predicting such detrimental effects of axial tension because of empirically determined parameters with safety factors. In this respect, several well-established theories for shear [3–5] are based not only on the force equilibrium, but on the failure kinematics. The former and latter respectively correspond to lower and upper bound solutions. The lower bound analysis is the basis of the shear design expression in most international codes. This lower bound is the reason underlying their inherent conservativeness, which is appropriate for designing new structures. For structural assessment of existing RC members, however, such conservativeness is of less importance than determining the actual bearing capacity [6].

Among the currently available theories, the Modified Compression Field Theory (MCFT) has provided a consistent framework to consider the influence of axial force and to facilitate its incorporation into various international codes and specifications. Nevertheless, the MCFT predictions might elicit some discrepancy with several test results of RC beams under axial tension [2]. Current understanding should be supplemented theoretically for rational shear assessment because the limitations of existing test results include laboratory-scale specimens without web reinforcement [7], despite recent progress [8, 9].

This paper presents a rational analysis based on the lower bound theorem. The analytical structure is based on the combined upper and lower bound analysis [10], which predicted the shear strengths of RC beams accurately with no axial force and no web reinforcement. The present work extends their original theory to consider the effectiveness of web reinforcement and the negative effects of axial tension. Rigorous formulation for shear failure is presented, including shear resisting mechanisms such as aggregate interlock and dowel action of longitudinal reinforcement under both force equilibrium and strain compatibility. The developed analysis is validated by comparison of its solutions with MCFT-based predictions and test results of three full-scale RC girders subjected to axial tension [7]. The notation used for this study is summarised in the Appendix.

2. Model Formulation

2.1. Analytical framework

In the theoretical framework of limit analysis [11], the exact solution lies between lower and upper bound solutions, for which the former and latter respectively satisfy force equilibrium and compatible patterns of failure, in addition to yield criteria. One therefore finds the exact solution by maximising the lower bound solutions. To derive shear strength with

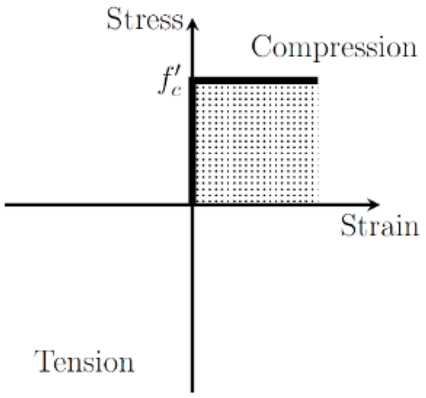

FIGURE 1. Constitutive law of concrete.

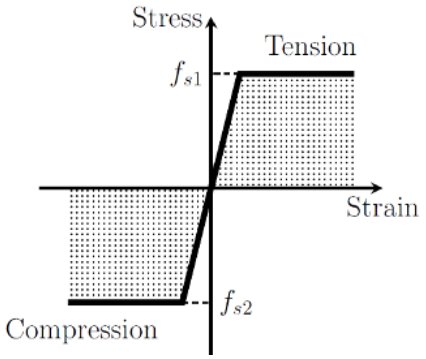

FIGURE 2. Constitutive law of steel reinforcement.

reasonable simplification, the following assumptions are introduced.

- Concrete and steel reinforcement are in a plane stress state.
- Perfect bonding exists between steel reinforcement and concrete.
- Concrete strength equal to over a compression zone; concrete behaves as a rigid - perfectly plastic material, as presented in Figure 2.
- Steel reinforcement behave as an elastic - perfectly plastic material, as shown in Figure 2.

It is noteworthy that the physical quantities such as forces, stresses and strains in compression are negative. Those denoted with a prime have positive compression.

2.2. FORCE EQUILIBRIUM

Figure 3 shows the free-body diagram with the shear resisting components against the external shear and axial tension force, respectively denoted as V and N. This equilibrium condition yields the following expressions, respectively, for vertical force, horizontal force, and moment.

$$V - V_c - F_d - F_w - b\int_t f \sin\theta \,\mathrm{d}t = 0 \qquad (1)$$

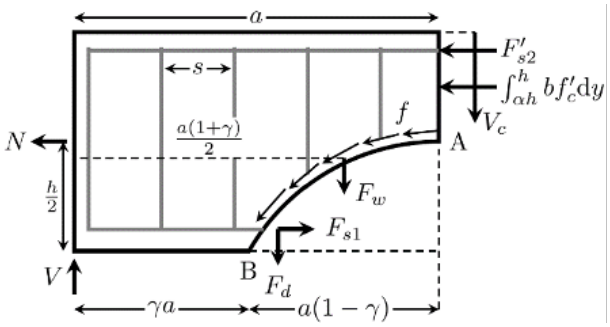

FIGURE 3. Free-body diagram.

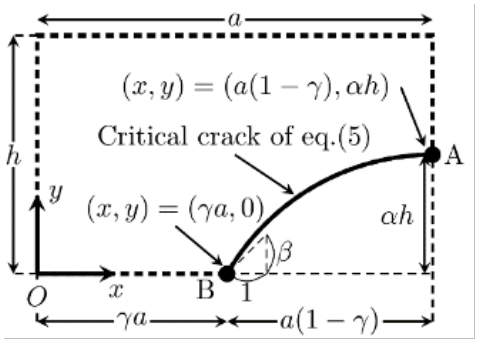

FIGURE 4. Critical crack shape.

$$\int_{\alpha h}^{h} bf'_c \,\mathrm{d}y - F_{s1} - F'_{s2} + N + b\int_t f\cos\theta \,\mathrm{d}t = 0 \qquad (2)$$

$$\begin{aligned}[\gamma a + \cot\beta\,(h-d_1)]\,F_d + (h-d_1)\,F_{s1} \;-\\ (h-d_2)\,F'_{s2} + \frac{a\,(1+\gamma)}{2}F_w + aV_c - \frac{h}{2}N \;-\\ \frac{h\,(1+\gamma)}{2}\int_{\alpha h}^{h} bf'_c \,\mathrm{d}y \;+\\ b\left(\int_t f\sin\theta\, x\,\mathrm{d}t - \int_t f\cos\theta\, y\,\mathrm{d}t\right) = 0\end{aligned} \qquad (3)$$

Therein, $\int_t \mathrm{d}t$ denotes the path integral from point A to B in Figure 3. One can replace these integrations with the following integrations with respect to x and y.

$$\int_t \cos\theta\,\mathrm{d}t = \int_{\gamma a}^{a}\mathrm{d}x, \qquad \int_t \sin\theta\,\mathrm{d}t = \int_0^{\alpha h}\mathrm{d}y \qquad (4)$$

Mathematical treatment of the path integral requires an expression for the critical crack shape shown in figure 4 on the $x-y$ coordinates.

$$y^2 = \frac{\alpha^2 h^2\,(x-a\gamma)}{a\,(1-\gamma)} \qquad (5)$$

Dividing equations 1, 2 and 3 respectively by $bd_1f'_c$ and $abd_1f'_c$, one obtains non-dimensionalised expressions as presented below.

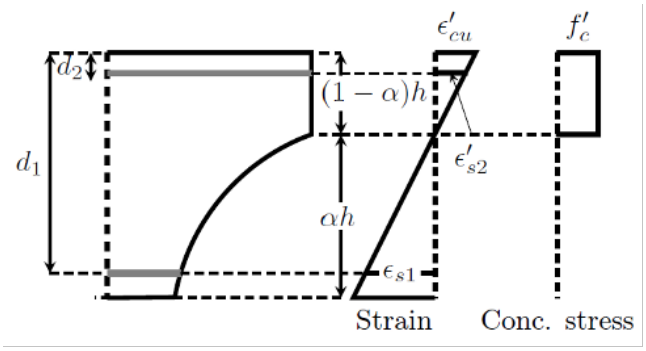

Figure 5. Strain compatibility.

$$v = (1-\alpha)\,\tau_c + \phi_{s1}\tau_s + \omega\phi_{sw}\sigma_w + \frac{\alpha}{\mu}\,\overline{f} \tag{6}$$

$$\frac{1-\alpha}{\mu} - \phi_{s1}\sigma_{s1} + \phi_{s2}\sigma_{s2} + n + \lambda\,(1-\gamma)\,\overline{f} = 0 \tag{7}$$

$$\begin{aligned}\left[\gamma + \cot\beta\left(\zeta - \frac{1}{\lambda}\right)\right]\tau_s\phi_{s1} + \left(\zeta - \frac{1}{\lambda}\right)\phi_{s1}\sigma_{s1} - \\ \left(\zeta - \frac{\delta}{\lambda}\right)\phi_{s2}\sigma_{s2} + \frac{1+\gamma}{2}\omega\phi_w\sigma_w + (1-\alpha)\,\tau_c - \\ \frac{\zeta}{2}n - \frac{\zeta}{2\mu}\left(1-\alpha^2\right) - \frac{\alpha}{3\mu}\,(1-4\gamma)\,\overline{f} = 0\end{aligned} \tag{8}$$

In those equations, the non-dimensional static variables are defined as shown below.

$$\begin{cases} v = \dfrac{V}{bd_1 f'_c},\ \ \sigma_{s1} = \dfrac{F_{s1}}{A_{s1}f_{s1}},\ \ \sigma_{s2} = \dfrac{F'_{s2}}{A_{s2}f_{s2}}, \\ \sigma_w = \dfrac{F_w}{A_{sw}f_{sw}},\ \ \tau_c = \dfrac{V_c}{bd_1 f'_c\,(1-\alpha)}, \\ \tau_s = \dfrac{F_d}{A_{s1}f_{s1}},\ \ n = \dfrac{N}{bd_1 f'_c},\ \ \overline{f} = \dfrac{f}{f'_c}. \end{cases} \tag{9}$$

Equation 6 is the objective function in this study. The non-dimensional shear strength of v is maximised with respect to the static variables.

2.3. Compatibility conditions

Though lower bound solutions do not require compatibility conditions, an inequality constraint for aggregate interlock $\left(\overline{f}\right)$ can be derived from strain compatibility. Figure 5 presents the strain compatibility on the cracked section. The assumption of Bernoulli-Euler beam (plane sections remain planar) yields the linear distribution of longitudinal strain. Those of bottom and top reinforcement are obtained respectively as shown below.

$$\varepsilon_{s1} = \frac{d_1 - (1-\alpha)\,h}{(1-\alpha)\,h}\,\varepsilon'_{cu} = 0.0035\left(\frac{\mu}{1-\alpha} - 1\right) \tag{10}$$

$$\varepsilon_{s2} = \frac{(1-\alpha)\,h - d_2}{(1-\alpha)\,h}\,\varepsilon'_{cu} = 0.0035\left(\frac{\delta\mu}{1-\alpha} - 1\right) \tag{11}$$

The neutral axis depth under the effect of axial tension is calculable by arranging Equation 6 with respect to $k = (1-\alpha)h/d_1$ as presented in the equation below.

$$\begin{aligned}k = &\frac{\varepsilon'_{cu}E_s}{f'_c}\left\{\frac{(\rho_{s1} + \delta\rho_{s2})\,\mu}{1-\alpha} - (\rho_{s1} + \rho_{s2})\right\} - \\ &\overline{f}\,\lambda\,(1-\gamma) - n\end{aligned} \tag{12}$$

Equation 12 gives an upper limit of the aggregate interlock in maximisation because k must be positive according to its definition.

2.4. Yield criterion and solution technique

The following von Mises yield criterion is introduced between τ_s and σ_{s1}.

$$3\tau_s^2 + \sigma_{s1}^2 = 1 \tag{13}$$

Although Hweé et al. [10] used another yield criterion for concrete, it need not be addressed in this study because the rigid - perfectly plastic behaviour is assumed. The complete set of equations enables the maximisation of the objective function of Equation 6 with respect to the six static variables $\left(\sigma_{s1},\ \sigma_{s2},\ \sigma_w,\ \tau_c,\ \tau_s,\ \text{and}\ \overline{f}\right)$. The possible ranges of those variables are presented as the following.

$$\begin{aligned}\sigma_{s1},\ \sigma_{s2},\ \sigma_w &\in \langle 0,\ 1\rangle \\ \tau_c,\ \tau_s,\ \overline{f} &\in \langle 0,\ \infty\rangle\end{aligned} \tag{14}$$

All of those expressions must be positive. The upper limits of $\sigma_{s1},\ \sigma_{s2},$ and σ_w and correspond with yielding of reinforcement. Although no upper limit is imposed on the others, Equation 7, 8, 12, and 13 render them physically admissible values.

Maximisation is performed using the optimisation algorithm of MATLAB [12], under the equality and inequality constraints listed in Table 1. All possible

Objective function	Equation 6
Equality constraints (force equilibrium)	Equation 7 and 8
Equality constraints (yield criterion)	Equation 13
Inequality constraints (neutral axis depth)	Equation 12 ≥ 0
Inequality constraints (yield criterion)	$3\tau_s^2 + \sigma_{s1}^2 \leq 1$

TABLE 1. List of constraints for optimisation.

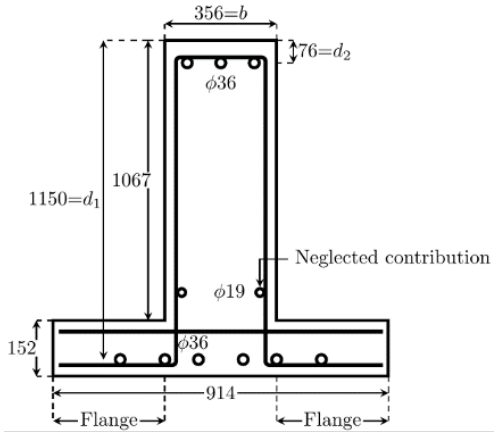

FIGURE 6. Cross-sectional details of inverted-T beams (unit: mm).

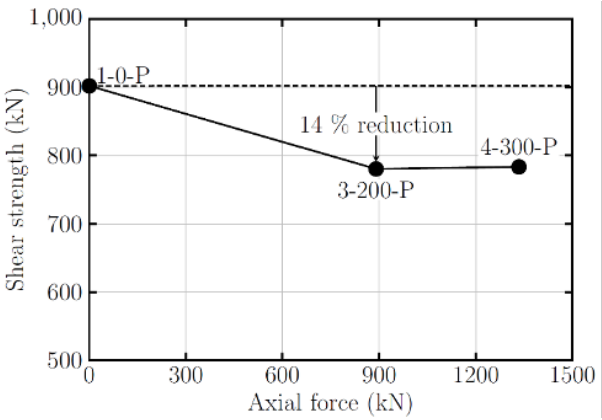

FIGURE 7. Shear strength dependence on applied axial force.

values of v are calculated within the following ranges of kinematic variables.

$$\begin{gathered} 1-\mu \leq \alpha \leq 1 \\ \frac{\alpha h}{a\,(1-\gamma)} \leq \beta \leq \infty \\ 0 \leq \gamma \leq 1 \end{gathered} \tag{15}$$

The lower limits of and stem respectively from the assumption that the longitudinal strain of bottom reinforcement in Equation 10 must be positive, and that the critical crack is directed upwards at $y = 0$ (Figure 3).

To obtain more optimal solution, the maximised solutions are then minimised with kinematic variables. The partial derivative of equation (6) with respect to determines whether the objective function is monotonically decreasing or increasing. The minimised shear strengths are calculable as presented below.

$$\frac{\partial v}{\partial \alpha} = -\tau_c + \frac{\overline{f}}{\mu} \tag{16}$$

$$\begin{cases} v_{ana} = \phi_{s1}\tau_s + \omega\phi_{sw}\sigma_w + \dfrac{\overline{f}}{\mu} \\ \left(\text{if } \dfrac{\partial v}{\partial \alpha} < 0,\ \ \alpha_{max} = 1 \text{ gives } v_{ana}\right) \\ v_{ana} = \mu\tau_c + \phi_{s1}\tau_s + \omega\phi_{sw}\sigma_w + \dfrac{1-\mu}{\mu}\,\overline{f} \\ \left(\text{if } \dfrac{\partial v}{\partial \alpha} > 0,\ \ \alpha_{max} = 1-\mu \text{ gives } v_{ana}\right) \end{cases} \tag{17}$$

3. RESULTS AND DISCUSSION

3.1. EXPERIMENT RESULTS

The analytical solutions have been compared with test results obtained for full-scale RC girders [7]. The studied girders had the inverted-T configuration (Figure 6) to support the deck in flexural tension. Figure 7 presents the detrimental effect of axial tension on shear strength. The axial force of 900 kN decreases the shear strength by 14%. The axial force magnitudes of 3-200-P and 4-300-P were found respectively to represent shrinkage-induced stress only, and both the shrinkage and temperature-induced stress. It is noteworthy that Smith et al. [7] tested seven specimens in all. The three specimens shown in figure 7 were extracted for model validation because the others included the use of cut-off bars and epoxy injected specimen, of which the contributions were not formulated.

3.2. MODEL VALIDATION

To calculate the shear strength by the developed analysis, static and kinematic constants were determined as listed respectively in Tables 2 and 3. These values were calculable using information referred from reports of the related literature [7]. The rectangular area of bd_1 in Figure 6 was used for calculation because the contributions of the flanges under flexural tension are negligible. In addition, the values of ε'_{cu}

	$n = \frac{N}{bd_1 f'_c}$	$\phi_{s1} = \frac{\rho_{s1} f_{s1}}{f'_c}$	$\phi_{s2} = \frac{\rho_{s2} f_{s2}}{f'_c}$	$\phi_w = \frac{\rho_{sw} f_{sw}}{f'_c}$
1-0-P	–	0.221	0.110	0.064
3-200-P	0.083	0.269	0.135	0.079
4-300-P	0.128	0.267	0.133	0.081

Table 2. Non-dimensional static constants.

	$\lambda = \frac{a}{d_1}$	$\zeta = \frac{h}{a}$	$\mu = \frac{d_1}{h}$	$\sigma = \frac{d_1}{d_2}$	$\omega = \frac{s}{d_1}$
1-0-P					
3-200-P	2.60	0.407	0.943	0.066	0.265
4-300-P					

Table 3. Non-dimensional kinematic constants.

	V_{exp}	v_{exp}	v_{ana}	V_{AASHTO}	$\frac{v_{ana}}{v_{exp}}$	$\frac{V_{AASHTO}}{V_{exp}+V_{dl}}$
	(kN)	(−)	(−)	(kN)	(−)	(−)
1-0-P	902	0.0773	0.0809	810	1.05	0.88
3-200-P	780	0.0814	0.0879	743	1.08	0.93
4-300-P	783	0.0835	0.0847	712	1.01	0.89

Table 4. Accuracy of the developed analysis.

and E_s in equation (12) are assumed respectively as 0.0035 and 200 kN/mm^2 because the original data were not found in the literature [7].

Table 4 presents comparisons among test results (V_{exp}), present analysis (v_{ana}), and MCFT-based prediction by AASHTO LRFD bridge design specification [13]. The analytical solutions show adequate accuracy (v_{ana}/v_{exp}) with specimens under axial tension (3-200-P and 4-300-P) and without axial tension (1-0-P). In all cases, the static variable of σ_w was equal to one when the optimisation terminated.

This value represents the yielding of web reinforcement, which was observed in the experiments as well. Furthermore, results demonstrate better agreement than the MCFT-based predictions, except for those for specimen 3-200-P. Although the analytical predictions of 3-200-P and 3-400-P show a consistent decrease of shear strength with the increase of applied axial force, no such tendency was observed in the experiment as presented in Figure 7. Further investigation about this discrepancy will be reported in another paper with a broad range of experimental data.

4. Conclusions

Shear strengths under the effect of axial tension loading were derived analytically based on the lower bound theorem. The theoretical basis treated the shear strength derivation as an optimisation problem under equality and inequality constraints obtained from force equilibrium, strain compatibility and yield criteria. Model validation showed good correspondence between experimental and analytical shear strengths without any regression functions and empirically determined parameters. The accuracy was an equal level with MCFT-based predictions. The generality of this formulation enables the consistent treatment of axial compression, and gives quantitative results of each shear component such as aggregate interlock of cracked concrete and dowel action of longitudinal reinforcement. Although further verification by comparison with a number of test results is necessary, the developed analysis might contribute to the provision of comprehensive understanding of shear behaviour under axial force, together with the MCFT [2] and other well-established theories [3–5]. Research is currently underway to extend this theory to axially compressed and tensioned beams without web reinforcement.

List of symbols

f'_c Concrete compressive strength
V External shear force
N External force of axial tension
V_c Shear component of uncracked concrete
F_w Shear component of web reinforcement
f Aggregate interlocking force per unit area
θ Inclination angle of critical crack to x-axis
F_d Dowel force of bottom reinforcement
F_{s1}, F_{s2} Longitudinal forces of bottom and top reinforcement, respectively
α Critical crack height divided by total depth

β Slope of critical crack at point B

γ Longitudinal distance between support and point B divided by shear span

a Shear span

b Web width

d_1 Effective depth

h Total depth

d_2 Distance between top reinforcement and upper perimeter of beams

s Spacing between adjacent web reinforcement

t Coordinate axis along critical crack

ω Spacing between adjacent web reinforcement divided by effective depth

μ Effective depth divided by total depth

λ Slenderness (shear span-to-depth) ratio

ζ Total depth divided by shear span

δ d1 divided by d2

k Neutral axis depth divided by effective depth

ε'_{cu} Ultimate compressive strain of concrete (0.0035)

E_s Modulus of elasticity of longitudinal reinforcement (200 GPa)

ρ_{s1}, ρ_{s2}, ρ_{sw} Reinforcement ratios of bottom, top and web reinforcement, respectively

A_{s1}, A_{s2}, A_{sw} Areas of bottom, top and web reinforcement, respectively

f_{s1}, f_{s2}, f_{sw} Yield strengths of bottom, top and web reinforcement, respectively

ε_{s1}, ε_{s2}, ε_{sw} Longitudinal strains of bottom and top reinforcement, respectively

ϕ_{s1}, ϕ_{s2}, ϕ_{sw} Reinforcement degrees of bottom, top and web reinforcement, respectively

Acknowledgements

Financial support from a Grant-in-Aid for Scientific Research from the Japan Society of Promotion of Science (19K15062) is greatly appreciated.

References

[1] R. C. Elstner, E. Hognestad, editors. Laboratory investigation of rigid frame failure. *Journal Proceedings*, **53**:637-668 1957.

[2] S. B. Bhide, M. P. Collins. Influence of axial tension on the shear capacity of reinforced concrete members. *Structural Journal* **86**(5):570-81, 1989.

[3] Y. Yang, J. den Uijl, J. Walraven. Critical shear displacement theory: on the way to extending the scope of shear design and assessment for members without shear reinforcement. *Structural Concrete* **17**(5):790-8, 2016. https://doi.org/10.1002/suco.201500135.

[4] A. Muttoni, M. Fernández Ruiz. Shear strength of members without transverse reinforcement as function of critical shear crack width. *ACI Structural Journal* **105**(2):163-72, 2008. https://doi.org/10.14359/19731.

[5] B. I. Mihaylov, E. C. Bentz, M. P. Collins. Two-Parameter Kinematic Theory for Shear Behavior of Deep Beams. *ACI Structural Journal*, **110**(3):447-56, 2013.

[6] Fib. Shear and Punching Shear in RC and FRC Elements (Lausanne: International Federation for Structural Concrete), *fib Bulletin* **57**:268, 2010.

[7] SM. T. Smith, D. A. Howell, M. A. T. Triska, et al. Effects of axial tension on shear-moment capacity of full-scale reinforced concrete girders. *ACI Structural Journal* **111**(1):211, 2014. https://doi.org/10.14359/51686534.

[8] D. Fernández-Montes, E. González Valle, E. Díaz Heredia. Influence of axial tension on the shear strength of floor joists without transverse reinforcement. *Structural Concrete* **16**(2):207-20, 2015. https://doi.org/10.1002/suco.201400063.

[9] D. T. Pham, B. Fouré, N. Pinoteau, et al. Influence of axial tension on the shear strength of RC beams without stirrups. *Structural Concrete* **22**(2):1037-53, 2020. https://doi.org/10.1002/suco.202000077.

[10] K. H. Tan, A. Hasegawa, F. Nishino. Determination of Ultimate Shear Strength of Reinforced Concrete Beams without Web Reinforcement by a Combined Upper and Lower Bound Analysis. *Doboku Gakkai Ronbunshu* **1986**(368):23-33, 1986. https://doi.org/10.2208/jscej.1986.368_23.

[11] D. C. Drucker. On structural concrete and the theorems of limit analysis. *International Association for Bridge and Structural Engineering*, Division of Engineering, Brown University, p. 36, 1961.

[12] S. J. Chapman.MATLAB programming for engineers, CL Engineering, Toronto: Nelson Education, 2015.

[13] AASHTO. AASHTO LRFD Bridge Design Specifications, *7th ed. American Association of State Highway and Transportation Officials*, Washington, D.C., 2013.